sciendo

***MINERALOGIA**, 50, No 1-4: 34-68 (2019)*
DOI: 10.2478/mipo-2019-0003
www.Mineralogia.pl

MINERALOGICAL SOCIETY OF POLAND
POLSKIE TOWARZYSTWO MINERALOGICZNE

Original paper

Geochemistry, mineral chemistry and P-T evaluation of metasediments of Bahram-Gur complex, ES Sanandaj-Sirjan zone, Iran

Hadiseh Rahimi Sadegh[1], Hesam Moeinzadeh[1]*, Kazu Nakashima[2]

[1] *Department of Geology, College of Sciences, Shahid Bahonar University, Kerman, 76176, Iran*
[2] *Earth and Environmental Sciences Department, University Yamagata, Yamagata990, Japan*
** Corresponding author*
e-mail: hmoeinzadeh@uk.ac.ir

Received: *Januray 12, 2019*
Received in revised form: *December 12, 2019*
Accepted: *December 30, 2019*
Available online: *March 20, 2020*

Abstract. The Bahram-Gur area in the southeastern part of the Sanandaj – Sirjan metamorphic zone, contains metabasites and metasediments. The metasedimentary rocks are mainly garnet schists and garnet-staurolite schists that were metamorphosed under amphibolite facies conditions. The rocks consist of garnet ± staurolite, biotite, muscovite, chlorite and quartz. The geochemistry of the Bahram-Gur metasediments classifies them as quartziferous sedimentary rocks. The protoliths of the metasedimentary rocks were close to greywackes from an ensialic arc basin depositional setting, with a source comprising mostly mixture of acid and intermediate magmatic rocks in the upper continental crust. The metamorphic conditions of formation of the Bahram-Gur metasedimentary are investigated by geothermobarometric methods. The results show that the metasedimentary rocks formed at temperatures of 600-750°C and pressures of 5-7.5 kbar.

Key-words: Bahram-Gur area, Sanandaj-Sirjan Zone, metamorphic conditions, metasediments, geothermobarometry

1. Introduction

Mineralogical and geochemical research has increased our knowledge of the sedimentary origin, basin characteristics and tectonic evolution of sedimentary basins (Maas, McCulloch 1991; Degraaff-Surpless et al. 2002; Cope et al. 2005; She et al. 2006). Siliciclastic rocks are good tools for studying the sedimentary origin and tectonic environments of sedimentary basins (Dickinson 1970; Bhatia1 983; Dickinson 1985; Floyd,

Leveridge 1987; Roser, Korsch 1988). The sedimentary origin, especially those of active continental margins, is difficult to identify due to erosion and subsequent degradation. In such cycles, a study of related sedimentary rocks is a useful way of determining the origin of the rocks and the history of the active margins of ancient continents (Sun et al. 2008).

The main structures of the Sanandaj-Sirjan zone were formed during three important events, the subduction of the north-east part of the Arabian plate under the central Iranian plate, the formation of the ophiolite of the Sanandaj-Sirjan belts, and finally the continental collision between the two plates in the Miocene (Ghazi, Moazzen 2015). The evolution of the Sanandaj-Sirjan zone was controlled by the opening and closure of Neotethys in the southeastern margin of Gondwana (Alavi 1994; Mohajjel, Fergusson 2014). The rocks of this zone are strongly deformed and tectonized due to continental collision.

The closure of the Paleotethys basin in the north led to the opening of Neotethys (Berberian, King 1981; Berberian, Berberian 1981; Hooper et al. 1994). The formation and then the spreading of Neotethys ocean occurred from the Permian to Triassic. The rock sequences associated with extension of Neotethys are mainly late Triassic in the Sanandaj-Sirjan metamorphic zone. The subduction of the Tethys Ocean in the late Triassic to Cretaceous led to deformation, metamorphism, and discontinuity in the marginal sub-sequences, and then the deformation was completed (Mohajjel et al. 2003). According to Shahabpour (2005), the presence of the northern branch of Neotethys and its subduction, and eventually the collision of the island arc at the end of the Cretaceous, caused various episodes of metamorphism, deformation, and discontinuities.

Metasediments of the region are pelitic schists containing garnet ± staurolite, biotite, muscovite, chlorite and quartz. There has been no comprehensive study of the metasediments in the southeastern part of the Sanandaj -Sirjan zone. Determining the rock types and evolution of the metasediments and constraining their metamorphic conditions are important in understanding the geodynamics of the Sanandaj-Sirjan zone.

2. Geology of the study area

The Bahram-Gur area, with an extent of more than 150 km^2, is located at latitude 29° 12′ and 29 ° 28′ North and longitude 54° 18′ and 55° 50′ East, at 50 km NW of Gol-e-Gohar mine, Sirjan city, within the SE Sanandaj-Sirjan metamorphic zone.

The metamorphic rocks of the region include a series of rocks of igneous and sedimentary origin. The rocks of the study area were regionlly metamorphosed,resulting in different types of amphibolites, metasediments, metabasites, serpentinites, paragneisses, and meta-carbonates (Fig. 1).

The rocks were metamorphosed up to the amphibolite facies (Sabzehi 1997). They are Proterozoic to Mesozoic in age (Horton et al. 2008) and are overlain by Phanerozoic shallow-water sediments of passive margin type. The metasedimentary rocks along with amphibolites, gneisses and meta-carbonates form layers within the other rocks such as schists up to 5 m thick and with a general trend of N50E and dip of 35NW. All rocks are displaced by predominantly NW-SE and N-S trending faults, making it difficult to study the original stratigraphic relations (Fig. 2a). In these rocks, metamorphic zones and mineral assemblage were well developed under various metamorphic conditions and show clear reaction relationships. Among these rocks, garnet schists and garnet-staurolite schists have

been studied here to determine the conditions of metamorphism; they belong to two different subunits.

The garnet schists (HRS-17, HRS-2) are exposed in two parts of the north and east of the study area in a Triassic-age subunit. They are glossy with a gray color in the field. The schistosity in these rocks is formed of biotite, muscovite and chlorite orientation. Due to tectonic activity, these rocks were crushed such that the schistosity is not visible in the field (Fig. 2c).

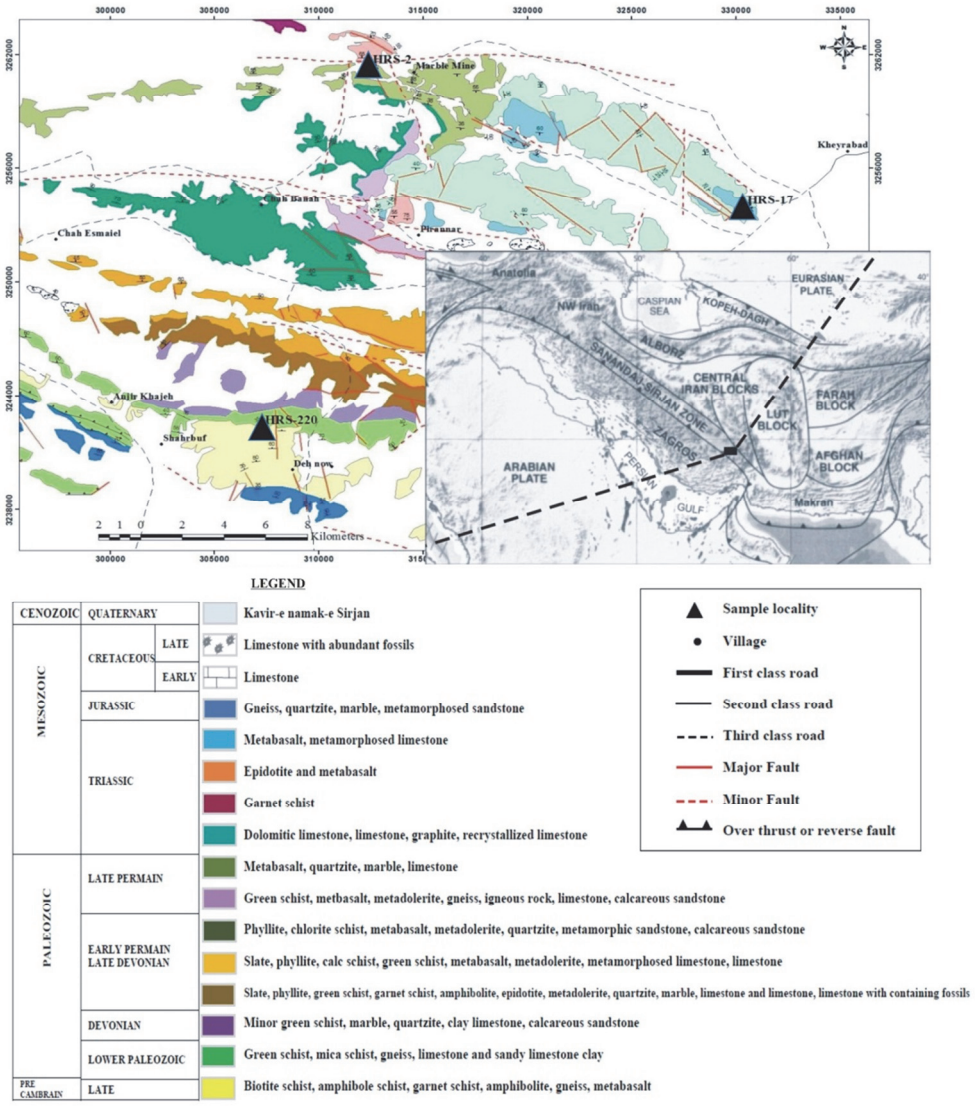

Fig. 1. Location of the study area in a map of Iranian structural units and a geological map of the Bahram Gur region of Sirjan (after Sabzehi 1997), along with i the location of the metasediment samples.

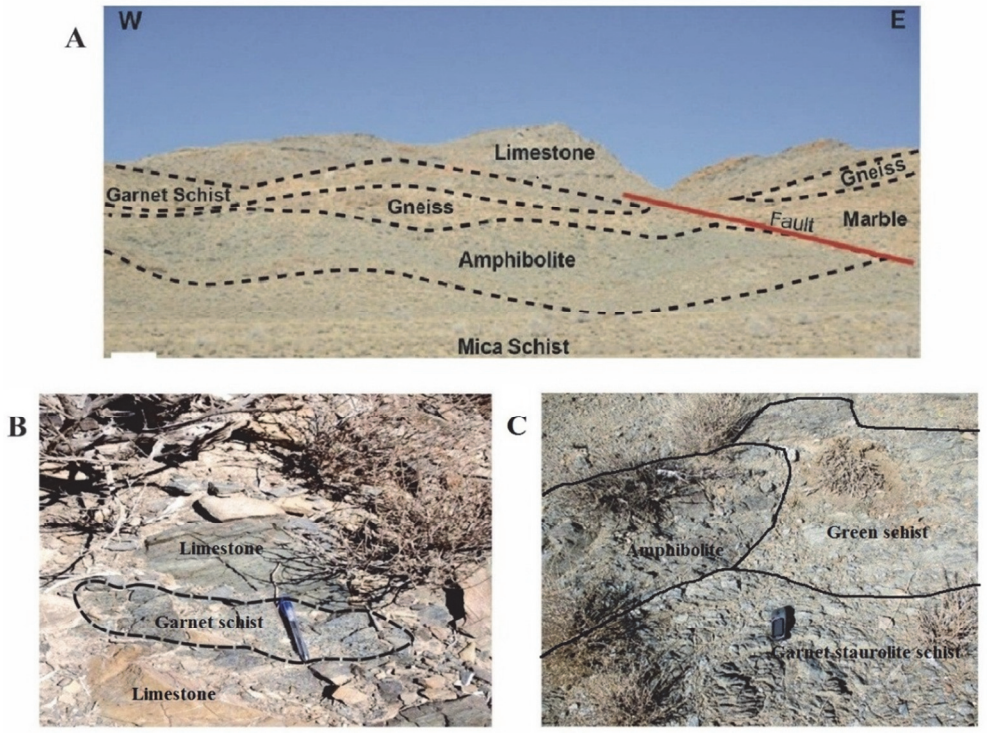

Fig. 2. a. Overview and field relationships of the main rock units in the area, b. Field characteristics of garnet-staurolite schists (HRS-220), C. Outcrop of garnet schist (HRS-17) in the area.

Garnet-staurolite schists (HRS-220) occur in the southern subunit of the area along with slates, phyllites, greenschists and amphibolites of lower Paleozoic age (Fig. 2b). These rocks are glossy and show a distinct schistosity due to the orientation of muscovite and biotite.

3. Petrography of the metasediments

Under the microscopic, the main minerals of the garnet schists (HRS-2) are garnet, quartz, muscovite, biotite, and chlorite and the minor phases are tourmaline, zircon, apatite and opaque minerals. Garnet occurs as inter-tectonic porphyroblasts and due to high amounts of inclusions is poikiloblastic. The garnet crystals are altered to biotite and chlorite at the rims and along crystal fractures. Iron oxides also fill the fractures.

The phyllosilicate minerals are mostly biotite, muscovite and chlorite. The primary biotite is oxidized and secondary chlorite resulting from alteration of biotite. Quartz in garnets mostly has wavy extinction and mosaic texture. The dominant textures in these rocks are porphyroblastic and lepidoblastic.

Two metamorphic phases S_0 and S_1 can be distinguished in the garnet schists. S_1 or S_e (the external schistosity) has been developed by quartz, muscovite and biotite, and relict of S_0 or S_i (the internal schistosity) by garnet, quartz and opaque minerals (Fig. 3a).

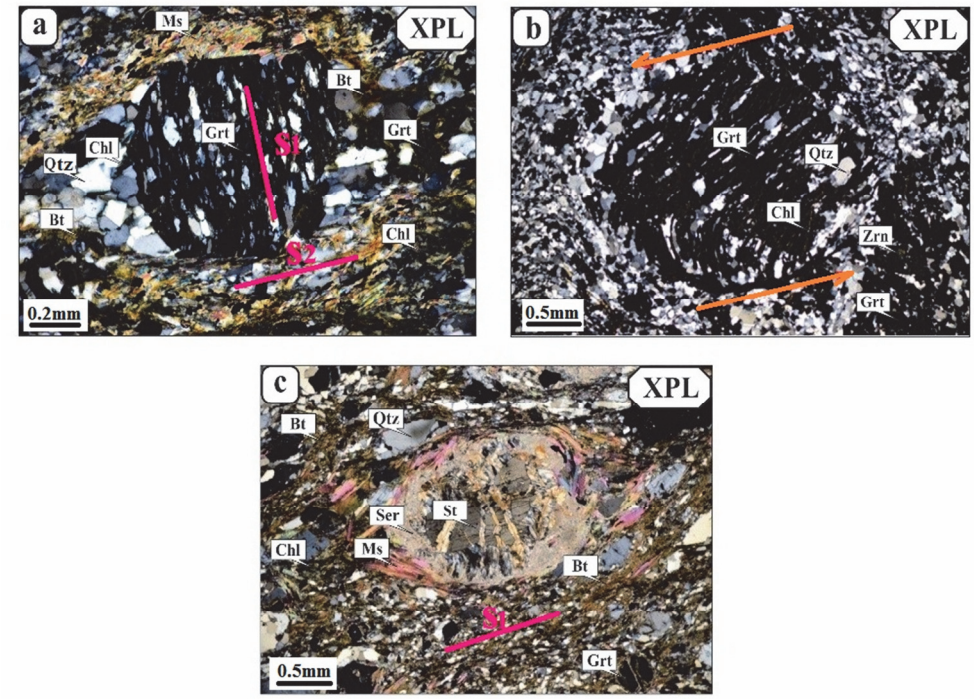

Fig. 3. a. Garnet schists in the east of the area as inter-tectonic porphyroblasts with poikiloblastic texture, b. Garnet schists in the northern part of the study area with snowball habit, c. Garnet-staurolite schist in the study area and coarse porphyroblasts broken staurolite, crystallized syn-tectonically. Abbreviations (Kretz, 1983): Grt: Garnet; St: Stuarolite; Bt: Biotite; Ms: Muscovite; Chl: Chlorite; Qtz: quartz; Zrn: Zircon.

The main minerals of the garnet schists (HRS-17) include garnet, quartz, muscovite and the minor phases are zircon, and opaque minerals. Snowball garnets are usually interspersed in their rotational state, but there are no disconnections between the inner-layer foliation with the background and the existence of a non-tangential pressure shadow, indicative of shear forces (Passchier, Trouw 2005), suggesting the simultaneous crystallization of S_1garnets (syn-tectonic), which have been rotated during formation (Barker 1990) (Fig. 3b).

The main minerals in the garnet-staurolite schists (HRS-220) are staurolite, garnet, muscovite, biotite, quartz and plagioclase, and the secondary minerals are chlorite, tourmaline and zircon.

Staurolite can be seen as coarse-grained porphyroblasts that are altering to sericite from the margins and secondary chlorites resulting from alteration of garnets that they are replaced in microfractures within the garnets (Fig. 3c).

The metamorphic phase S_1 is visible due to the orientation of the matrix minerals, muscovite, biotite, chlorite and quartz along with the foliation. Staurolite porphyroblasts are formed syntectonically and garnet porphyroblasts grew after the D_1 deformation, namely, post tectonic (Fig. 3c). The main texture of the rock is porphyroblastic.

4. Analytical Methods and the results

4.1. Mineral chemistry of metasediments

Mineral chemical analyses were performed on polished thin sections using an automated JEOL JXA-8900 electron probe micro-analyser (EPMA) at the EMS Laboratory of Yamagata University in Japan with an accelerating voltage of 15 kV, a beam current of 20 nA, a beam diameter of about 5 μm, detection limits of 0.05wt%, and a maximum 40 s counting interval. Data were processed by an online computer using the oxide ZAF in the XM-86 PAC program of JEOL. Analyses were made of plagioclase, garnet, staurolite, biotite, muscovite and chlorite. The results are presented in Tables 1 to 6.

4.1.1. Garnet

The average composition of the garnet in the garnet schists (HRS-2, HRS-17) is mainly in the form of almandine; the range of end-members of HRS-2 sample is $Alm_{72-81}Prp_{2-20}Sps_{0-3}$ Grs_{7-22} and the composition of HRS-17 is $Alm_{67-78}Prp_{3-5}Sps_{1-7}Grs_{16-22}$. Garnet staurolite schists (HRS-220) are mainly a solid solution between almandine and pyrope ($Alm_{61-64}Prp_{17-22}Sps_{11-13}$ Grs_{5-7}), both with a dominant composition of almandine (Table 1).

Figure 6 shows the variation in almandine - pyrope - grossular - spessartine and their zoning from margins to cores in different units of the study area.

In the garnet staurolite schist (HRS-220) the garnets belong to the almandine - pyrope series and are homogeneous so that the amount of almandine from core to the margin is high but the amount of pyrope is low, and spessartine and grossular also increase (Fig. 4a).

The major composition of garnet in the garnet schist sample HRS-17, from margin to crystal core, is almandine. The largest amount of garnet is related to the almandine, so that does not change from the core to margin of the almandine, pyrope, grossular, and spessartine and does not show zoning (Fig. 4b).

The analyses of garnet in the garnet schist sample HRS-2, from the margin to core of the crystal, is almost that of almandine, and shows zoning with the amount of almandine and grossular increasing and that of pyrope decreasing from the margin to the core of the crystal. The remaining crystals show a constant trend without zoning (Fig. 4c).

As seen in Figure 5, the percentage of almandine and pyrope in the garnet-staurolite schists is more than the other garnet end members, while in the garnet schists, garnet has higher almandine contents.

TABLE 1

EPMA analysis of garnets in the metasediments

Samples	HRS-220			HRS-2					HRS-17				
Points	220-1-1	220-1-2	220-1-4	2-3-2	2-3-5	2-3-8	2-4-3	22-4-6	17-1-5	17-1-8	17-1-10	17-2-8	17-2-10
Positon	core	mid	rim	core	mid	rim	mid	rim	core	mid	rim	mid	rim
SiO_2	38.66	38.79	38.49	38.66	37.42	38.09	39.80	38.39	38.48	38.28	38.23	38.85	36.79
TiO_2	0.00	0.06	0.00	0.10	0.13	0.16	0.13	0.16	0.11	0.08	0.07	0.01	0.05
Al_2O_3	21.67	22.40	21.74	20.60	21.00	22.41	21.51	19.16	18.36	19.56	20.75	21.16	20.71
Cr_2O_3	0.00	0.04	0.00	0.00	0.00	0.00	0.05	0.00	0.00	0.13	0.44	0.06	0.07
Fe_2O_3	0.00	0.00	0.11	0.00	1.22	0.00	0.00	0.00	0.00	0.00	0.00	0.00	1.15
FeO	27.77	28.44	28.93	33.32	34.52	33.91	29.42	34.14	33.12	33.20	33.66	29.36	30.86
MnO	4.82	4.96	5.86	0.23	0.23	0.10	0.29	0.12	1.46	0.40	0.32	3.20	2.04
MgO	5.67	5.43	4.50	1.72	0.89	1.02	0.92	1.51	0.82	1.13	1.15	0.71	1.06
CaO	1.80	1.94	2.46	6.56	6.66	6.39	7.02	5.09	7.16	6.35	5.37	7.59	7.19
Total	100.39	102.05	102.08	101.20	102.06	102.09	99.16	98.56	99.51	99.13	100.00	100.94	99.91
Structural formulas based on 12 Oxygens													
Si	3.04	3.00	3.00	3.07	2.97	3.00	3.21	3.15	3.13	3.12	3.09	3.10	2.97
Ti	0.00	0.00	0.00	0.01	0.01	0.01	0.01	0.01	0.01	0.00	0.00	0.00	0.00
Al	2.01	2.04	2.00	1.93	1.97	2.08	2.05	1.85	1.76	1.69	1.98	1.99	1.97
Cr	0.00	0.00	0.00	0.00	0.00	0.00	0.00	0.00	0.00	0.00	0.03	0.00	0.00
Fe^{3+}	0.00	0.00	0.01	0.00	0.07	0.00	0.00	0.00	0.00	0.00	0.00	0.00	0.07

Samples	HRS-220			HRS-2					HRS-17				
Points	220-1-1	220-1-2	220-1-4	2-3-2	2-3-5	2-3-8	2-4-3	22-4-6	17-1-5	17-1-8	17-1-10	17-2-8	17-2-10
Fe^{2+}	1.82	1.84	1.88	2.21	2.29	2.24	1.99	2.34	2.25	2.39	2.28	1.96	2.09
Mn	0.32	0.33	0.39	0.02	0.02	0.01	0.02	0.01	0.10	0.05	0.02	0.22	0.14
Mg	0.66	0.63	0.52	0.20	0.11	0.12	0.11	0.19	0.10	0.12	0.14	0.08	0.13
Ca	0.15	0.16	0.20	0.56	0.57	0.54	0.61	0.45	0.62	0.55	0.47	0.65	0.62
Total	8.00	8.00	8.00	8.00	8.00	8.00	8.00	8.00	7.96	7.93	8.00	8.00	8.00
almandine	61.61	62.33	62.85	73.99	76.94	77.04	72.91	78.51	73.15	75.79	78.45	67.36	70.08
pyrope	22.42	21.22	17.43	6.82	3.53	4.12	4.08	6.21	3.29	4.61	4.76	2.90	4.30
grossular	5.13	5.42	6.81	18.61	18.27	18.52	22.16	14.92	20.21	18.57	15.77	22.25	20.14
spessartine	10.84	11.01	12.88	0.52	0.51	0.24	0.73	0.29	3.27	1.03	0.76	7.44	4.69
uvarovite	0.00	0.01	0.00	0.00	0.00	0.00	0.04	0.00	0.00	0.02	0.22	0.04	0.04
andradite	0.00	0.00	0.02	0.00	0.68	0.00	0.00	0.00	0.00	0.00	0.00	0.00	0.71
Ca-Ti Gt	0.00	0.01	0.00	0.06	0.07	0.08	0.09	0.08	0.08	0.05	0.04	0.00	0.03

TABLE 2

EPMA analysis of staurolite in the metamorphic rocks

Samples	HRS-220		
Positions	220-5-1	220-5-2	220-5-3
SiO_2	28.20	28.54	28.55
TiO_2	0.63	0.68	0.62
Al_2O_3	53.68	53.69	53.85
Cr_2O_3	0.08	0.00	0.03
FeO	11.65	11.37	11.59
MnO	0.48	0.59	0.57
MgO	1.40	1.31	1.32
CaO	0.00	0.03	0.01
K_2O	0.02	0.03	0.02
Total	96.13	96.23	96.55
Structural formulas based on 8 Oxygens			
Si	3.941	3.977	3.969
Ti	0.066	0.071	0.065
Al	8.841	8.820	8.824
Cr	0.009	0.000	0.004
Fe^{++}	1.361	1.325	1.347
Mn	0.057	0.069	0.067
Mg	0.291	0.273	0.274
Ca	0.000	0.004	0.001
K	0.003	0.005	0.003
Total	14.569	14.544	14.553
XFe	0.796	0.795	0.798
XMg	0.170	0.164	0.162

XFe= Fe(Mg+Fe+Mn+Zn)
XMg= Mg(Mg+Fe+Mn+Zn)

TABLE 3

EPMA analysis of the plagioclase in the metasedimentary rocks

Samples	HRS-220					
Positions	220-1-1	220-1-2	220-1-3	220-1-4	220-1-5	220-1-6
SiO_2	62.51	62.75	62.71	62.38	62.17	62.80
TiO_2	0.06	0.00	0.00	0.00	0.01	0.00
Al_2O_3	23.93	24.29	24.01	24.14	23.93	24.10
Cr_2O_3	0.10	0.00	0.08	0.00	0.06	0.00
FeO	0.02	0.00	0.01	0.00	0.04	0.05
MnO	0.00	0.03	0.02	0.03	0.00	0.06
MgO	0.01	0.00	0.00	0.03	0.01	0.00
CaO	5.83	5.76	5.43	5.74	5.51	5.14
BaO	0.00	0.00	0.00	0.00	0.00	0.01
Na_2O	7.92	7.74	7.94	7.36	7.49	8.01
K_2O	0.08	0.08	0.04	0.06	0.07	0.07
Total	100.46	100.64	100.24	99.74	99.29	100.24
Structural formulas based on 8 Oxygens						
Si	2.776	2.784	2.791	2.800	2.801	2.793
Ti	0.002	0.000	0.000	0.000	0.000	0.000
Al	1.253	1.270	1.259	1.277	1.271	1.263
Cr	0.004	0.000	0.003	0.000	0.002	0.000
Fe^{2+}	0.001	0.000	0.000	0.000	0.002	0.002
Mn	0.000	0.001	0.001	0.001	0.000	0.002
Mg	0.001	0.000	0.000	0.002	0.001	0.000
Ca	0.277	0.274	0.259	0.276	0.266	0.245
Ba	0.000	0.000	0.000	0.000	0.000	0.000
Na	0.682	0.666	0.685	0.641	0.654	0.690
K	0.004	0.004	0.002	0.004	0.004	0.004
Total	5.00	5.00	5.00	5.00	5.00	5.00
An	28.76	29.01	27.35	29.98	28.77	26.07
Ab	70.78	70.54	72.42	69.64	70.79	73.49
Or	0.46	0.45	0.23	0.39	0.44	0.43

TABLE 4

The results of EPMA analysis of biotite in the metasedimentary rocks

Samples	HRS-220									
Positions	h220-1-5	h220-1-6	h220-2-9	h220-2-10	h220-2-11	h220-5-1-1	h220-5-1-2	h220-5-1-3	h220-5-2-2	h220-5-2-3
SiO_2	35.77	35.40	36.12	36.26	35.98	35.57	36.40	35.52	34.75	36.30
TiO_2	1.39	1.75	1.38	1.24	1.11	1.28	1.24	1.37	1.19	1.25
Al_2O_3	17.70	17.50	17.62	17.03	17.51	18.05	16.60	17.60	18.52	17.24
FeO	17.81	17.48	16.72	17.15	18.38	18.73	17.75	18.50	18.66	17.82
MnO	0.21	0.11	0.18	0.08	0.26	0.15	0.13	0.13	0.23	0.17
MgO	12.45	11.92	13.20	12.59	13.55	13.25	12.22	11.99	13.16	12.43
CaO	0.11	0.17	0.05	0.10	0.18	0.00	0.02	0.03	0.08	0.04
Na_2O	0.10	0.11	0.12	0.08	0.27	0.10	0.12	0.09	0.11	0.15
K_2O	8.68	9.35	8.48	8.96	6.35	7.42	9.33	8.34	7.36	8.73
BaO	0.10	0.18	0.06	0.13	0.04	0.14	0.05	0.06	0.05	0.19
F	0.54	0.26	0.52	0.40	0.17	0.23	0.42	0.34	0.13	0.27
Cl	0.10	0.18	0.18	0.08	0.20	0.08	0.19	0.11	0.19	0.07
Cr_2O_3	0.00	0.16	0.00	0.00	0.01	0.05	0.06	0.02	0.04	0.06
NiO	0.00	0.06	0.10	0.03	0.03	0.00	0.14	0.00	0.02	0.05
Li_2O*	0.71	0.61	0.81	0.86	0.77	0.66	0.90	0.64	0.42	0.86
H_2O*	3.69	3.77	3.70	3.75	3.86	3.87	3.71	3.75	3.85	3.84
Subtotal	99.36	99.01	99.23	98.75	98.67	99.57	99.27	98.49	98.76	99.46
O=F,Cl	0.25	0.15	0.26	0.19	0.11	0.12	0.22	0.17	0.10	0.13

Samples	HRS-220									
Positions	h220-1-5	h220-1-6	h220-2-9	h220-2-10	h220-2-11	h220-5-1-1	h220-5-1-2	h220-5-1-3	h220-5-2-2	h220-5-2-3
Total	99.11	98.86	98.97	98.56	98.55	99.45	99.05	98.32	98.66	99.34
Structural formulas based on 22 Oxygens										
Si	5.40	5.38	5.42	5.49	5.40	5.33	5.51	5.41	5.26	5.46
Al^{iv}	2.60	2.62	2.58	2.51	2.60	2.67	2.49	2.59	2.74	2.54
Al^{vi}	0.55	0.52	0.54	0.53	0.50	0.52	0.48	0.57	0.57	0.52
Ti	0.16	0.20	0.16	0.14	0.13	0.14	0.14	0.16	0.14	0.14
Cr	0.00	0.02	0.00	0.00	0.00	0.01	0.01	0.00	0.00	0.01
Fe	2.25	2.22	2.10	2.17	2.31	2.35	2.25	2.36	2.36	2.24
Mn	0.03	0.01	0.02	0.01	0.03	0.02	0.02	0.02	0.03	0.02
Mg	2.80	2.70	2.95	2.84	3.03	2.96	2.76	2.72	2.97	2.79
Ni	0.00	0.01	0.01	0.00	0.00	0.00	0.02	0.00	0.00	0.01
Li*	0.43	0.37	0.49	0.52	0.47	0.40	0.55	0.39	0.26	0.52
Ca	0.02	0.03	0.01	0.02	0.03	0.00	0.00	0.01	0.01	0.01
Na	0.03	0.03	0.03	0.02	0.08	0.03	0.03	0.03	0.03	0.04
K	1.67	1.81	1.62	1.73	1.22	1.42	1.80	1.62	1.42	1.68
Ba	0.01	0.01	0.00	0.01	0.00	0.01	0.00	0.00	0.00	0.01
OH*	3.72	3.83	3.71	3.79	3.87	3.87	3.75	3.81	3.89	3.86
F	0.26	0.13	0.25	0.19	0.08	0.11	0.20	0.17	0.06	0.13
Cl	0.02	0.05	0.05	0.02	0.05	0.02	0.05	0.03	0.05	0.02
Total	19.94	19.95	19.94	19.99	19.80	19.85	20.05	19.87	19.80	19.99
Al total	3.15	3.14	3.12	3.04	3.10	3.19	2.96	3.16	3.31	3.06

Samples	HRS-220									
Positions	h220-1-5	h220-1-6	h220-2-9	h220-2-10	h220-2-11	h220-5-1-1	h220-5-1-2	h220-5-1-3	h220-5-2-2	h220-5-2-3
Fe/Fe+Mg	0.45	0.45	0.42	0.43	0.43	0.44	0.45	0.46	0.44	0.45

TABLE 5

EPMA Analysis Results of the muscovite in the metasedimentary rocks

Samples	HRS-2			HRS-220		
Positions	h2-2-1	h2-2-2	h2-2-3	h220-5-4	h220-5-5	h220-5-6
SiO_2	46.12	46.76	46.11	46.83	46.11	48.12
TiO_2	0.32	0.21	0.37	0.76	0.43	0.32
Al_2O_3	33.82	34.52	34.45	33.03	32.39	31.80
FeO	1.41	1.24	2.28	2.41	4.50	3.18
MnO	0.00	0.00	0.03	0.03	0.00	0.05
MgO	0.77	0.68	0.91	0.84	1.76	1.47
CaO	0.11	0.22	0.10	0.04	0.08	0.04
Na_2O	0.77	0.87	0.84	0.32	0.22	0.32
K_2O	9.21	8.30	8.69	8.93	8.19	8.06
BaO	0.15	0.08	0.17	0.22	0.45	0.22
F	0.15	0.00	0.24	0.00	0.25	0.17
Cl	0.00	0.01	0.00	0.02	0.06	0.04
Cr_2O_3	0.10	0.15	0.06	0.08	0.10	0.00
NiO	0.04	0.00	0.06	0.00	0.00	0.00
H_2O*	4.34	4.45	4.35	4.43	4.29	4.37
Subtotal	97.29	97.49	98.66	97.95	98.83	98.14
O=F,Cl	0.06	0.00	0.10	0.00	0.12	0.08
Total	97.22	97.49	98.56	97.94	98.71	98.06
Structural formulas based on 11 Oxygens						
Si	6.27	6.29	6.20	6.33	6.25	6.48
Al^{iv}	1.73	1.71	1.80	1.67	1.75	1.52
Al^{vi}	3.69	3.77	3.66	3.59	3.42	3.52
Ti	0.03	0.02	0.04	0.08	0.04	0.03
Cr	0.01	0.02	0.01	0.01	0.01	0.00
Fe	0.16	0.14	0.26	0.27	0.51	0.36
Mn	0.00	0.00	0.00	0.00	0.00	0.01
Mg	0.16	0.14	0.18	0.17	0.36	0.29
Ca	0.02	0.03	0.01	0.01	0.01	0.01
Na	0.20	0.23	0.22	0.08	0.06	0.08
K	1.60	1.42	1.49	1.54	1.42	1.38
Ba	0.01	0.00	0.01	0.01	0.02	0.01
OH*	3.94	4.00	3.90	4.00	3.88	3.92
F	0.06	0.00	0.10	0.00	0.11	0.07
Cl	0.00	0.00	0.00	0.00	0.01	0.01
Total	17.88	17.77	17.88	17.77	17.85	17.70
Al total	5.42	5.48	5.46	5.26	5.17	5.05
Fe/Fe+Mg	0.51	0.51	0.58	0.62	0.59	0.55

TABLE 6

EPMA analysis of chlorite in the metasedimentary rocks

Samples	h2-2-5	h2-2-6	h2-4-1	h2-4-3	h17-1-3	h17-2-1	h17-2-2	h220-2-12
SiO_2	26.68	26.84	26.62	26.48	23.27	24.49	27.05	27.12
TiO_2	0.10	0.10	0.00	0.00	0.01	0.04	0.04	0.26
Al_2O_3	20.76	20.36	19.67	20.36	16.58	22.49	19.59	19.01
Cr_2O_3	0.01	0.10	0.01	0.11	0.00	0.00	0.02	0.06
Fe_2O_3	1.87	2.56	2.84	3.43	0.00	2.30	2.87	0.00
FeO	25.76	28.53	29.94	29.13	41.82	35.96	32.82	20.21
MnO	0.00	0.00	0.00	0.00	0.05	0.00	0.01	0.24
MgO	10.58	8.73	6.48	6.54	4.35	3.53	3.93	19.00
NiO	0.00	0.07	0.06	0.03	0.03	0.00	0.00	0.15
CaO	0.18	0.25	0.18	0.13	0.41	0.10	0.22	0.07
Na_2O	0.01	0.05	0.04	0.00	0.07	0.00	0.08	0.08
K_2O	0.84	0.11	0.36	0.05	0.23	0.06	0.97	0.77
BaO	0.09	0.03	0.00	0.02	0.04	0.00	0.09	0.00
F	0.00	0.00	0.00	0.08	0.00	0.00	0.00	0.14
Cl	0.03	0.01	0.02	0.00	0.04	0.00	0.00	0.10
H_2O*	11.10	11.06	10.73	10.72	10.09	10.80	10.73	11.34
Subtotal	97.99	98.81	96.96	97.06	96.99	99.77	98.42	98.54
O=F,Cl	0.01	0.00	0.01	0.03	0.01	0.00	0.00	0.08
Total	97.98	98.81	96.95	97.03	96.98	99.77	98.42	98.46
Structural formulas based on 28 Oxygens								
Si	5.702	5.768	5.880	5.813	5.464	5.403	5.963	5.587
Al^{iv}	2.298	2.232	2.120	2.187	2.536	2.597	2.037	2.413
Al^{vi}	2.983	2.967	3.056	3.142	2.099	3.293	3.123	2.241
Ti	0.016	0.017	0.000	0.000	0.001	0.006	0.007	0.040
Cr	0.002	0.016	0.002	0.018	0.001	0.000	0.004	0.010
Fe^{3+}	0.301	0.414	0.472	0.567	0.000	0.382	0.476	0.000
Fe^{2+}	4.604	5.127	5.531	5.348	8.419	6.635	6.051	3.532
Mn	0.000	0.000	0.000	0.000	0.010	0.000	0.002	0.041
Mg	3.372	2.797	2.135	2.141	1.524	1.162	1.290	5.836
Ni	0.000	0.013	0.011	0.006	0.005	0.000	0.000	0.024
Ca	0.041	0.058	0.043	0.030	0.102	0.024	0.051	0.015
Na	0.004	0.040	0.034	0.000	0.067	0.000	0.065	0.066
K	0.457	0.061	0.202	0.026	0.139	0.032	0.547	0.406
Ba	0.015	0.005	0.000	0.004	0.007	0.000	0.015	0.000
F	0.000	0.000	0.000	0.106	0.000	0.000	0.000	0.176
Cl	0.021	0.007	0.017	0.000	0.033	0.000	0.001	0.069
OH*	15.979	15.993	15.983	15.894	15.967	16.000	15.999	15.755
Total	35.794	35.516	35.487	35.282	36.374	35.533	35.631	36.212
Fe/Fe+Mg	0.593	0.665	0.738	0.734	0.847	0.858	0.835	0.377
Mg/Mg+Fe	0.423	0.353	0.278	0.286	0.153	0.149	0.176	0.623

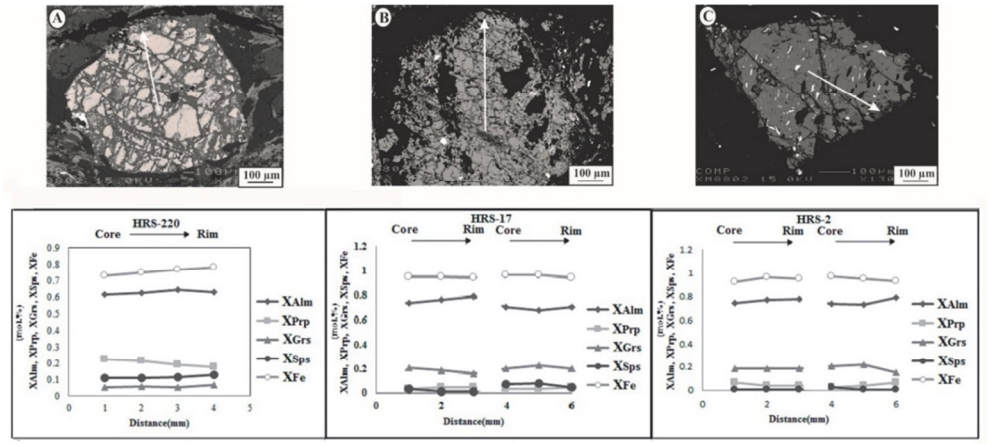

Fig. 4. Variations in the almandine, pyrope, grossular and spessartine contents from the core to margin in garnet from different rock types; a. Garnet-staurolite schist HRS-220, b. Garnet schist HRS-17, C. Garnet schist HRS-2.

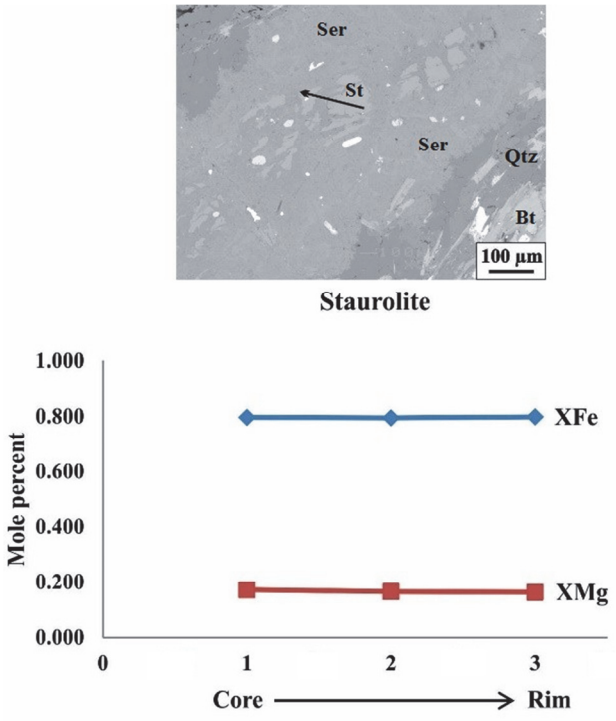

Fig. 5. Compositional changes from margin to core in staurolite.

4.1.2. Staurolite

Staurolite shows many different sizes. The results of the analysis show that the Fe, Mg concentrations from the core to margin do not change. The XFe content in these minerals is 0.79% and the XMg content is 0.17% (Table 2, Fig. 5).

4.1.3. Feldspar

The plagioclase is homogenous, only one analysis (Table 3, HRS-220-1-6) shows a slightly higher albite content and generally the amount of albite exceeds anorthite (Fig. 6).

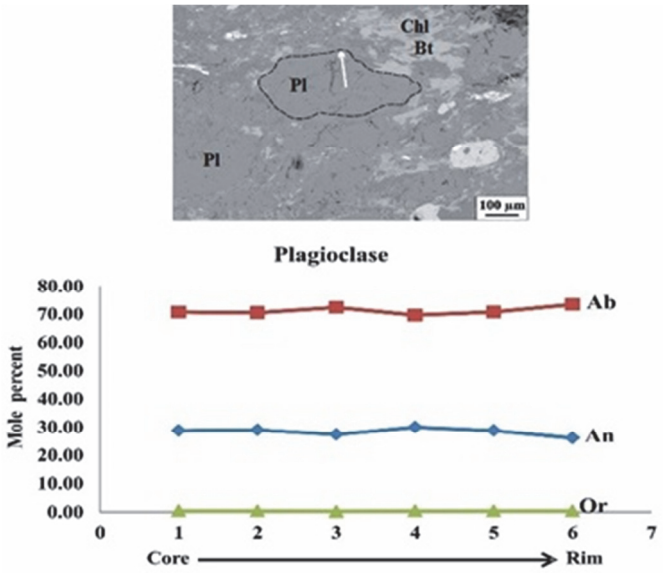

Fig. 6. The compositional changes from core to margin in plagioclase in the metasediments.

4.1.4. Biotite

Biotite is one of the most abundant minerals in the studied rocks. It crystallized in two stages. The first generation, along with muscovite and chlorite, are the main minerals in the metamorphic rocks of the region, and the second generation is a large crystal in the rock. An electron microprobe analysis of coarse-grained biotite in sample HRS-220 shows an eastonite to siderophyllite compound (Table 4, Fig. 7).

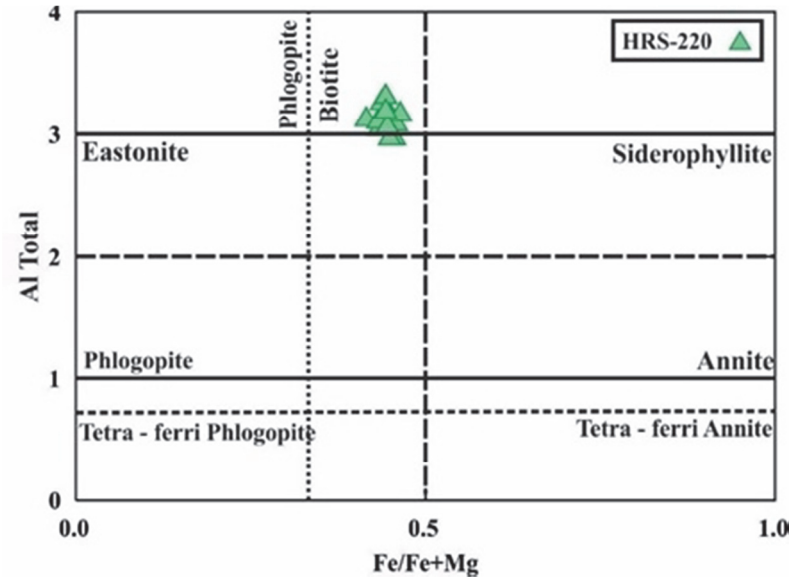

Fig. 7. The analysed biotite in the metasediments in Fe/(Fe + Mg) versus Al Total diagram (Rieder et al. 1998).

4.1.5. Muscovite

The other mineral in the studied sample is white mica; the EPMA results are given in Table 5. Muscovite is widely seen in the metasediments. A first generation, along with biotite and chlorite, is in the main foliation of the metamorphic rocks. A second generation is characterized by large porphyroblasts with a single direction, and crystallized in the main foliation. The third generation is a product of the progressive metamorphism of t sericite from the staurolites, so they are concentrated around and inside staurolite. The compositions of white micas from metasediments are shown on the FeO_T–Al_2O_3 diagram of Miyashiro (1973) where they plot in the field of the Chlorite-Biotite-Almandine Zone (Fig. 8). The mean values of the Fe/Fe+Mg content of muscovites observed in the presence of staurolite and garnet in HRS-220 and HRS-2 samples are 0.59 and 0.53, respectively (Table 5).

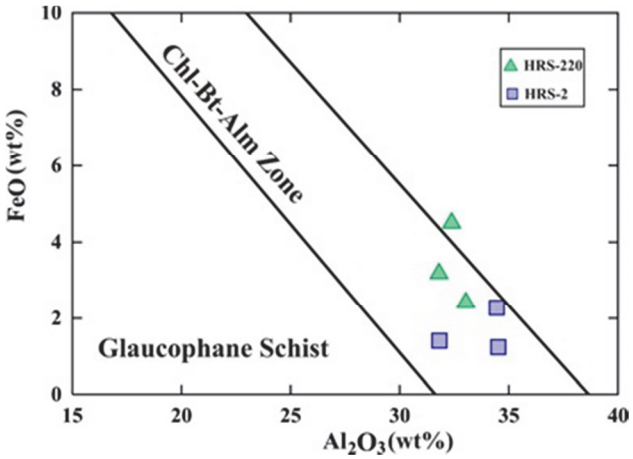

Fig. 8. The chemical composition of muscovite in the Miyashiro diagram (1973).

4.1.6. Chlorite

Based on the results of the chlorite point analysis (Table 6), the Fe/(Fe+Mg) ratio in sample HRS-220 is 0.37 and the Si content is 5.58 apfu; chlorites in the sample HRS-2 has Fe/(Fe+Mg) = 0.54-0.82 and Si content = 5.2-5.8 apfu; chlorites in sample HRS-17 has Fe/(Fe+Mg) = 0.83-0.86 and a Si content of 5.4-5.9 apfu which leads to the classification of chlorites as pycnochlorite, brunsvigite-ripidolite and brunsvigite-daphnite, respectively (Deer et al. 1996; Fig. 9). At increasing degrees of metamorphism, the XFe of chlorites decreases (Table 6). Chlorite from garnet staurolite schist in the garnet and staurolite zone have XFe of about 0.37.

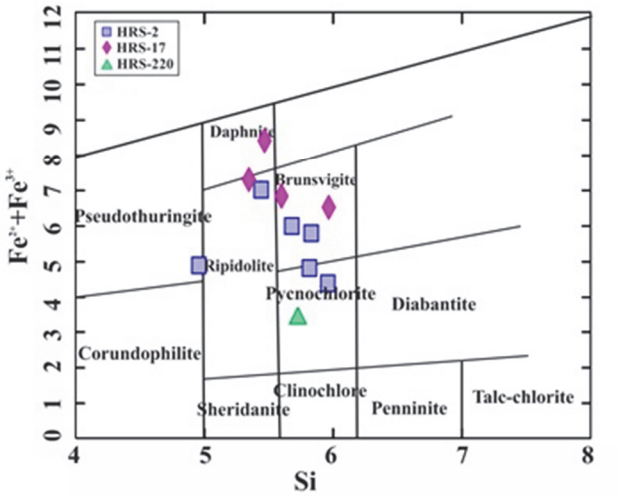

Fig. 9. The composition of the chlorites in the metasedimentary rocks in the diagram of Deer et al. (1996)

4.2. Phase equilibria in afm projection

Figure 12 shows a Summary of Chemographic Diagrams AFM for metasediment rocks.

The presence of chlorite, muscovite, biotite and garnet in low grade metamorphosed rocks (paragenesis [1]; chemographic diagrams of Figure 10; a):

[1] Grt + Bt + Chl + Ms + Pl + Qtz

Suggests that garnet probably was produced by the following dewatering reactions (reactions1, 2):

(1) Chl + Ms = Grt + Bt + Chl + H_2O, (2) Chl + Ms = Grt + Bt + Qtz + H_2O

Reaction (1) and (2) occurred in the equivalent epidote amphibolite facies.

The existence of garnet and staurolite with chlorite, muscovite, plagioclase and quartz in the field (paragenesis [2] and [3]; chemographic diagrams of Figure 10; b):

[2] St + Grt + Bt + Ms + Pl + Qtz, [3] St + Bt + Ms + Pl + Qtz

Reaction (3) suggests that formation of staurolite occurred in the equivalent lower amphibolite facies.

(3) Grt + Ms + Chl = St + Bt + Qtz + H_2O

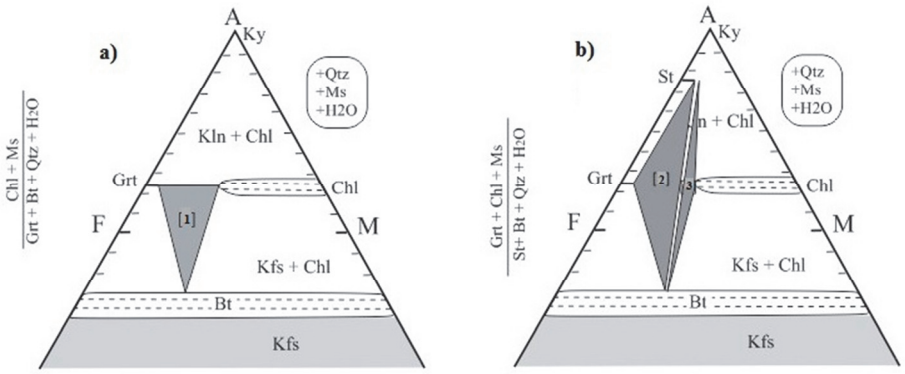

Fig. 10. Chemographic Diagrams AFM for: a) garnet schist, b) garnet staurolite schist. Lines indicate reactive phases. The numbers in the bracket introduce paragenesis.

4.3. Geochemistry and tectonic environment of the metasediments

The whole rock chemistry of metasediments can be used to determine the type of primary sedimentary rock and the accurate equilibrium minerals. For this purpose, three metasediments were selected as representative samples and were analysed by XRF-ICP / OES-ICP / MS methods at the Activation Laboratories Ltd (ACTLABS), Ancaster, Ontario, Canada. The concentrations of 10 major oxides, 45 minor elements, and LOI are reported in Table 7.

TABLE 7

Chemical analysis of the major, minor and rare elements of the metasediments

Samples	Major, Minor and Rare earths elemants																							
HRS-2	SiO_2	Al_2O_3	$Fe_2O_3^{(T)}$	$FeO^{(T)}$	MnO	MgO	CaO	Na_2O	K_2O	TiO_2	P_2O_5	LOI	Total	Mg#										
	63.7	15.9	9.92	8.93	0.05	1.13	1.37	0.31	3.17	2.69	0.1	1.93	100	18.4										
	Ti	Sc	Be	V	Ba	Sr	Y	Zr	Cr	Co	Ni	Cu	Zn	Ga	Ge	As	Rb	Nb	Mo	Ag	In	Sn	Sb	Cs
	0.4	14	2	174	368	88	41	579	90	14	40	30	80	27	2	12	68	64	< 2	0.8	< 0.2	8	0.7	2
	La	Ce	Pr	Nd	Sm	Eu	Gd	Tb	Dy	Ho	Er	Tm	Yb	Lu	Hf	Ta	W	Tl	Pb	Bi	Th	U		
	56.2	119	13.2	51.3	11.3	1.94	9.4	1.5	8.4	1.6	4.5	0.63	4.3	0.71	14	4.4	4	0.3	10	< 0.4	14.9	3		
HRS-17	SiO_2	Al_2O_3	$Fe_2O_3^{(T)}$	$FeO^{(T)}$	MnO	MgO	CaO	Na_2O	K_2O	TiO_2	P_2O_5	LOI	Total	Mg#										
	70.1	8.17	14.57	13.11	0.21	1.36	1.95	0.06	0.16	2.13	0.19	1.61	101	15.6										
	Ti	Sc	Be	V	Ba	Sr	Y	Zr	Cr	Co	Ni	Cu	Zn	Ga	Ge	As	Rb	Nb	Mo	Ag	In	Sn	Sb	Cs
	0.32	15	< 1	139	43	26	45	976	250	46	100	60	110	9	2	37	7	28	2	1.2	< 0.2	< 1	0.6	< 0.5
	La	Ce	Pr	Nd	Sm	Eu	Gd	Tb	Dy	Ho	Er	Tm	Yb	Lu	Hf	Ta	W	Tl	Pb	Bi	Th	U		
	48.1	101	11.5	44.2	9.2	1.75	8.2	1.3	7.5	1.5	4.4	0.65	4.4	0.74	21.4	2.1	3	< 0.1	< 5	< 0.4	24.8	7.3		
HRS-220	SiO_2	Al_2O_3	$Fe_2O_3^{(T)}$	$FeO^{(T)}$	MnO	MgO	CaO	Na_2O	K_2O	TiO_2	P_2O_5	LOI	Total	Mg#										
	62.2	15.5	6.64	5.97	0.07	3.93	2.53	3.3	1.83	0.85	0.18	3.04	100	54										
	Ti	Sc	Be	V	Ba	Sr	Y	Zr	Cr	Co	Ni	Cu	Zn	Ga	Ge	As	Rb	Nb	Mo	Ag	In	Sn	Sb	Cs
	0.13	16	2	121	375	243	30	196	150	19	50	70	120	18	1	< 5	63	8	< 2	< 0.5	< 0.2	2	0.6	1.8
	La	Ce	Pr	Nd	Sm	Eu	Gd	Tb	Dy	Ho	Er	Tm	Yb	Lu	Hf	Ta	W	Tl	Pb	Bi	Th	U		
	30	60.5	7.13	28	6.1	1.47	5.7	0.9	5.5	1.1	3.2	0.48	3.2	0.51	4.9	0.8	2	0.3	< 5	< 0.4	10.3	2		

The metasediments have 62-70wt% SiO_2. The abundance of Al_2O_3 is 8-16wt%, Fe_2O_3 varies between 6.6- 14.5wt% and MgO is 0.048-0.2wt%, the amount of TiO_2 is 0.8-0.6wt% and the abundance of MnO is less than 1wt% (Table 7).

The analysis of metasediment sample HRS-2 shows high SiO_2, Al_2O_3 and low Fe_2O_3 (total), MgO, CaO and Na_2O and high TiO_2, K_2O concentrations (Table 7).

The analysis of metasediment sample HRS-17 has high SiO_2 and Fe_2O_3 (total) and TiO_2 and low amounts of Al_2O_3, MgO, CaO, Na_2O and K_2O (Table 7).

The analysis of metasediment sample HRS-220 ahows low Fe_2O_3 (total) and TiO_2 and high SiO_2, Al_2O_3, MgO, CaO and Na_2O (Table 7).

The distribution of TiO_2 and Ni in the metasediments displays magmatic trends and plots in the magmatogenic greywacke field (Floyd et al. 1989; Fig. 11). This indicates a derivation from a magmatic source probably of acidic composition, and this is confirmed by a plot of La/Th vs. Hf (Floyd, Laveridge 1987; Fig. 12). On the other hand, these rocks in a Th/Sc-La/Sc diagram (Totten et al. 2000; Fig. 13) plot as derived from a rather mixed acid-intermediate arc source.

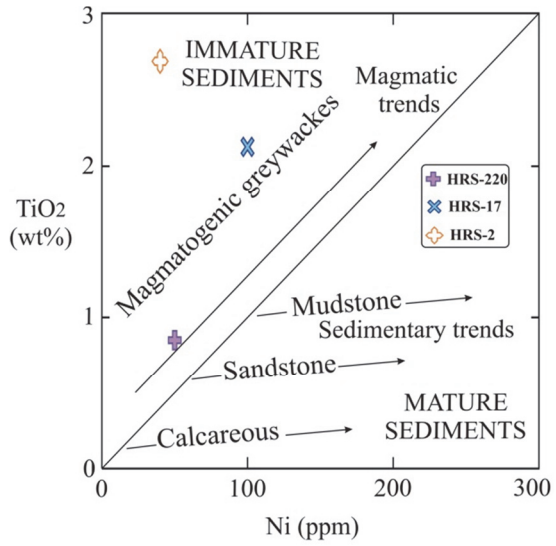

Fig. 11. TiO_2-Ni diagram for the Bahram-Gur Metasedimentary rocks testifying to their derivation from a magmatic precursor of predominantly acidic composition. Trends and fields taken from Floyd et al. (1989).

In order to determine the tectonic setting of the metasediments, the minor and trace element data are used. Trace elements have been used to discriminate effectively between ocean island arc (OIA), continental island arc (CIA), active continental margin (ACM) and passive margin (PM). On the Th-La-Sc and Co-Th-Zr/10 ternary diagrams, the metasediments of the Bahram-Gur complex plots within continental island arc settings (Bhatia, Crook, 1986; Fig.14 a,b).

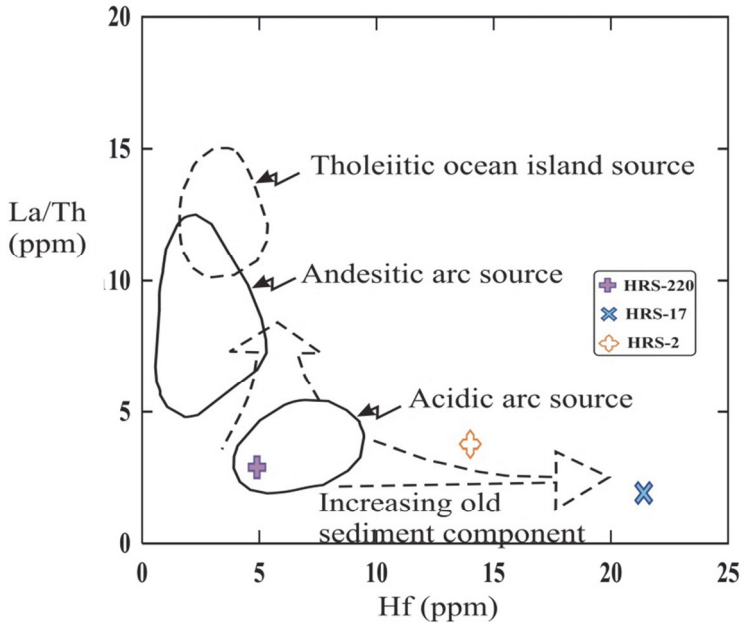

Fig. 12. Discrimination diagram Hf vs. La/Th for the Bahram-Gur metasedimentary rocks indicating derivation from an acidic arc source (fields after Floyd and Leveridge 1987).

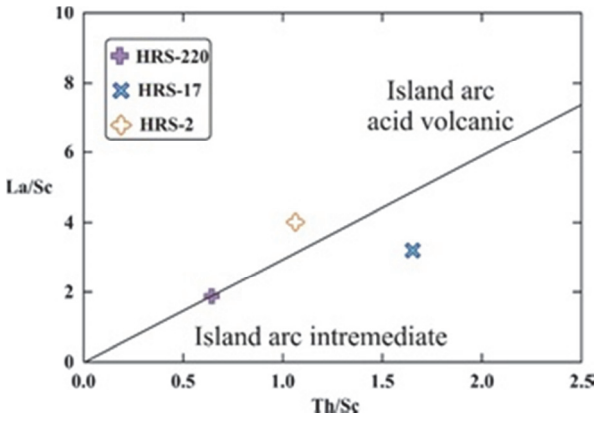

Fig. 13. Diagram Th/Sc vs. La/Sc (Totten et al. 2000) for the metasedimentary rocks from the Bahram-Gur complex.

The chondrite-normalized plots of the rare earth elements (REE) (Fig, 15a) generally show higher concentrations of light REE (LREE) than heavy REE (HREE) with a negative Eu-anomaly similar to that of the upper continental crust (UCC; McLennan 2001). The UCC-normalized plots of the REE show that most of the elements are comparable to the upper continental crust (UCC) composition (Fig. 15b).

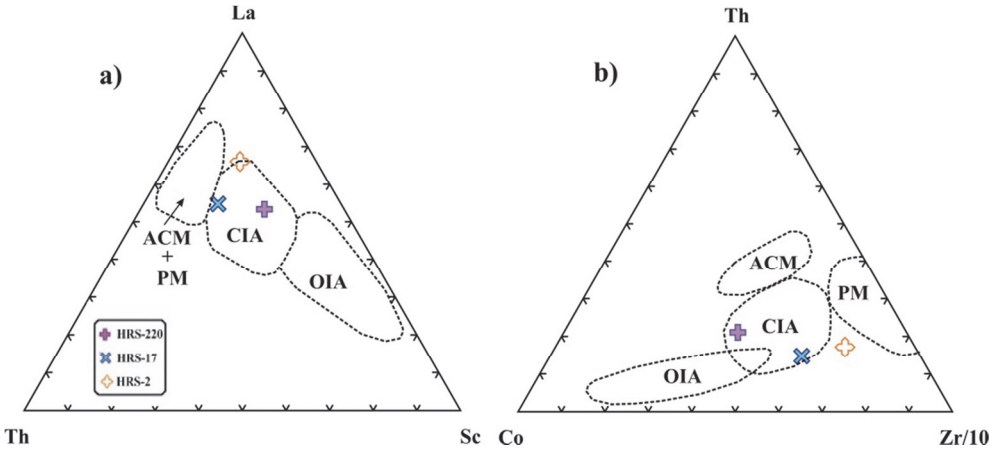

Fig. 14. a: The Th-La-Sc and b: Co-Th-Zr/10 tectonic discrimination ternary diagram. Fields after (Bhatia and Crook, 1986). (OIA: ocean island arc, CIA: continental island arc, ACM: active continental margin and PM: passive margin.)

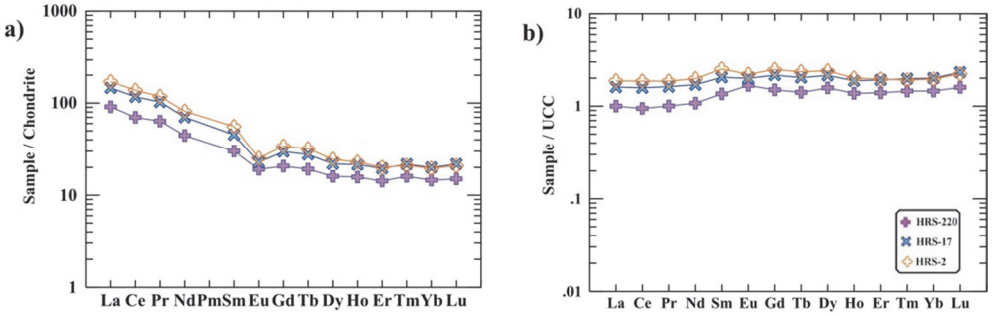

Fig. 15. REE patterns for the metasediment samples. (a) Chondrite-normalized REE plots showing UCC pattern, (b) UCC-normalized REE patterns is almost similar to UCC. Sources: chondrite (Sun, McDonough 1989), UCC (Taylor, McLennan, 1985).

5. Geothermobarometry

The basis of determining the temperature and pressure of minerals according to their chemical composition is based on the assumption that the mineral assemblage of each rock is formed under equilibrium conditions.

5.1. Garnet-biotite thermometer

This method of thermometry is based on the exchange of cationic iron and magnesium between homogeneous garnet and biotite, according to the following reaction (Thompson

1976; Holdaway, Lee 1977; Hodges, Spear1982; Perchuk, Lavrenteva 1983; Ferry, Spear1987; Dasgupta et al. 1991; Bhattacharya et al. 1992a, 1992b):

$Mg_3Al_2Si_3O_{12} + KFe_3AlSi_3O_{10}(OH)_2 = Fe_3Al_2Si_3O_{12} + KMg_3KAlSi_3O_{10}(OH)_2$

The results of garnet -biotite thermometry, from different calibrations, are presented in Table 8 by varying Fe and Mg contents in the core and the margin of the pair of garnets and biotite in the metasediments. The temperatures obtained from this thermometer are 635 to 810°C.

TABLE 8

Results of Garnet-Biotite Thermometry in the Garnet-Staurolite schist

Calibration Samples	Bhattachary a et al. (1992) HW	Bhattachary a et al. (1992) GS	Dasgupta et al.(1991)	Ferry and Spear (1987)	Hodges and Spear (1982)	Perchuk and Lavrenteva (1983)	Thompson (1976)	Holdaway and Lee (1977)
HRS-220 Garnet Staurolite Schist	692.54	698.98	787.18	789.05	810.53	687.19	750.97	711.07
	682.16	687.53	762.95	767.13	789.84	677.36	735.64	698.23
	652.01	655.15	724.63	709.35	731.48	650.41	694.37	663.42
	637.29	639.41	709.41	679.43	707.47	635.83	672.49	644.81

At about 510°C, garnet of almandine type and staurolite can form by reaction of chlorite and muscovite (Spear 1993; Bucher, Ferry 1994; Bucher, Grapes 2011).

The first appearance of staurolite and garnet in the metsediments represents the transition from greenschist facies to amphibolite facies. At the beginning of the amphibole facies, the temperature is slightly higher than 500°C (Bucher, Ferry 1994).

5.2. Garnet - Plagioclase-Biotite-Muscovite-Quartz Barometry (GPBMQ)

The homogeneous Garnet + Plagioclase + Biotite + Muscovite + Quartz assemblage is stable over a wide range of metasedimentary compositions and at a wide range of pressure and temperature. Pressure evaluation using pure transient reactions:

Grs + Prp + Ms = 3An + Phl & Grs + Alm + Ms = 3An + Ann

Which is possible in these coexisting minerals (Hoisch 1991). The calculated pressure for the metasedimentary sample HRS-220, obtained by using Fe end-members, is from 5.4 to 6.1 kbar, and based on the magnesium bearing end-members of the reaction is 6.9 to 7.7 kbar. A summary of the results of barometry is presented in Table 9.

It is expected that the two garnet and staurolite minerals in the rock containing minerals rich of Al and Fe^{+2} were formed from chlorite, muscovite and biotite breakdown.

TABLE 9

Barometric results of the Garnet-Staurolite schist

Samples	HRS-220			
Geobarometers	Pressure(kbar)			
GPMB-Mg Grs + Prp + Ms = 3An + Phl	7.6	7.6	6.9	7.4
GPMB-Fe Grs + Alm + Ms = 3An + Ann	6.0	5.9	5.4	6.1

5.3. Ti in biotite geothermometry

The Ti content in biotite is known to be a function of temperature variations in metamorphic rocks (Engel, Engel 1960; Kwak 1968; Robert1976; Dymek 1983; Patino Douce 1993).

Factors affecting the amount of Ti in biotite not only are related to temperature variations, but also to pressure, the composition of the biotite crystals and the associated mineral assemblage (Dymek 1983; Henry, Guidotti 2002)

This method is suggested for studying the thermodynamic conditions of peraluminous metasedimentary rocks at low to moderate pressures (Henry et al. 2005). Henry et al. (2005) formulated the thermometry as T (°C) = {[Ln (Ti) + 2.3594 + 1.7283 (X_{Mg})3] / (4.6482 × 10-9)} 0.333.

In which the number of Ti atoms calculated in the structural formula (in terms of a.p.f.u.) of biotite is based on 22 oxygen atoms and X_{Mg} is Mg / (Mg + Fe).

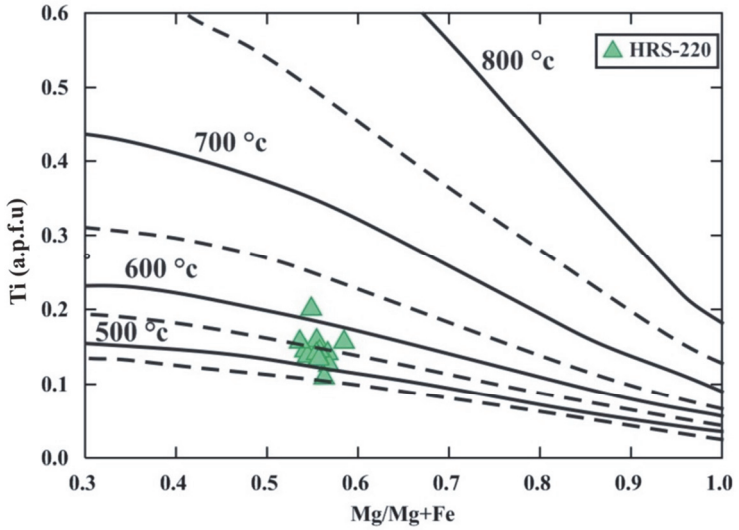

Fig. 16. Ti in biotite thermometry results (Henry et al. 2005)

This equation is for 1.00 - Ti = 0.04 - 0.60 a.p.f.u., X_{Mg} = 0.275 and T = 480 - 800°C (with an approximate error of ± 24°C) (Henry et al. 2005). The metamorphic temperatures obtained by Ti thermometry for garnet staurolite schist samples, are 454 and 602°C, respectively (Fig. 16).

5.4. Geothermobarometry by PT-Quick set

PT-Quick is a convenient ©MS Windows program for the estimation of equilibrium parameters (temperatures, pressures, oxygen fugacities) for mineral parageneses using methods of classical geothermobarometry, i.e. by independent expressions and algorithms ("tools") developed by different authors.

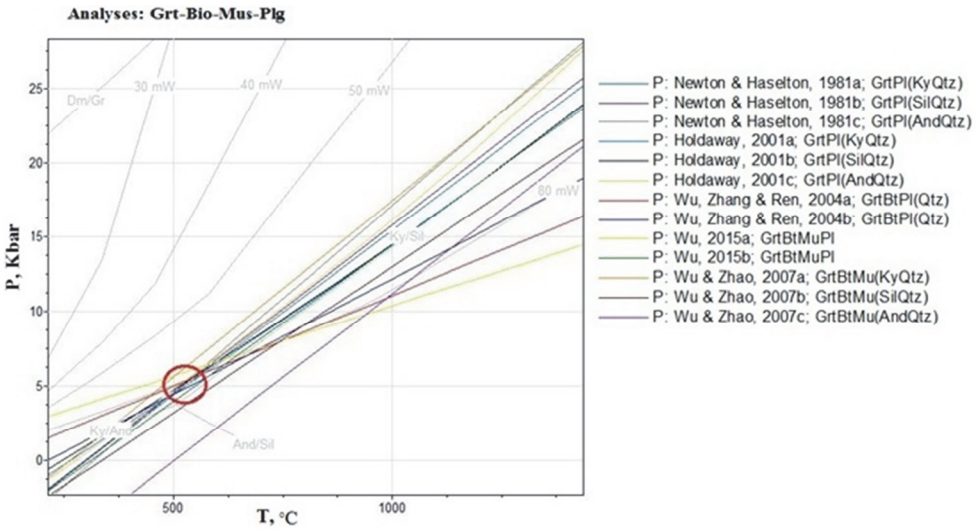

Fig. 17. A plot of pressure vs. temperature estimates for metasediments, Equilibration pressures (P) were estimated using the Grt–Bt-Ms-Pl barometer of Wu (2015 a,b), Wu, Zhao (2007 a,b,c), Wu et al. (2004 a,b), Holdaway (2001) and Newton, Haselton (1981).

The P-T values were calculated using the PT-Quick software provided by D. Dolvio-Dobrovolsky. The P-T estimates were also obtained by combinations of other thermometers and barometers to screen our P-T set for erratic values: garnet, biotite, muscovite and plagioclase barometry (Wu 2015a, 2015b; Wu, Zhao 2007,; Wu et al. 2004; Holdaway 2001; Newton, Haselton 1981; Fig. 17). The ranges of P-T values are 5-6 kbar and 650-700°C in this study.

5.5. Geothermobarometry by Thermocalc software

For the thermobarometry of the studied metasediments we used multiple equilibrium curves. The P-T conditions during metamorphism were determined by using standard geothermal-barometric methods and the Thermocalc thermodynamic program (version 2.4;

update 1995) (Holland & Powell, 1985). Thermocalc calculations are done in Equation 1 by selecting pressure and temperature values.

$$0 = \Delta G0(r)1,T + (P-1)((\Delta Vs + \Delta(\alpha V)(T-298)) - \Delta(\beta VP/2) + niRTln\tilde{f}i + RTlnK$$

The intersection of multiple equilibrium curves determines the temperature and pressure. The paragenesis of the studied rocks as Grt+ St+ Bt+ Ms+ Chl+ Qtz has the highest number of metamorphic minerals in mineralogical equilibrium. The activities of the end-members of garnet, biotite, muscovite and staurolite used in the Thermocalc program were calculated by the AX program of Holland and Powell (1998). Assuming that all solute minerals are pure end-members and assuming uniform activity for the soluble (such as garnet and staurolite) and pure phases (such as quartz), the equilibrium reactions were calculated by Thermocalc and plotted on PT diagrams (Fig. 18).

Thus, the calculated temperature and pressure for the metasediments are 600-700°C and 6-7.5 kbar, respectively.

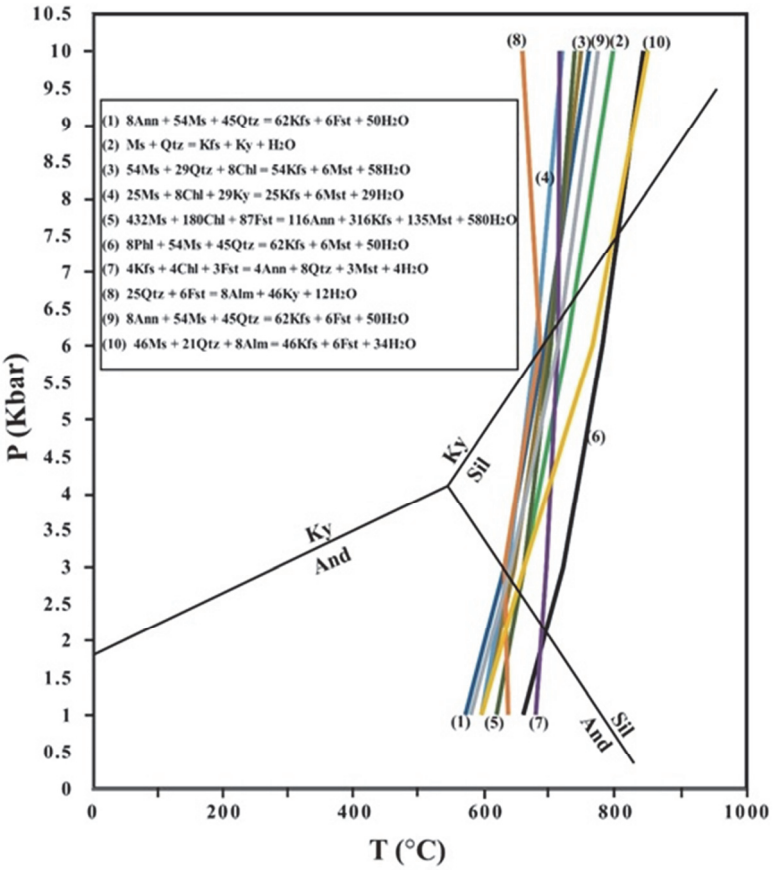

Fig. 18. Estimation of the pressure and temperature of Bahram-Gur metamorphic complex using a set of metamorphic reactions (thermocalc). The pressure of the metasediments of Bahram-Gur complex is 6 to 7.5 kbar and the temperature is from 600 to 700°C. Abbreviations (Kretz, 1983): Grt: Garnet; Alm: Almandine; Fst: Fe-Stuarolite; Mst: Mg-Stuarolite; Ms: Muscovite; Phl: Phlogopite; Chl: Chlorite; Ky: Kyanite; Kfs: K-feldspar; Ann: Annite; Qtz: quartz.

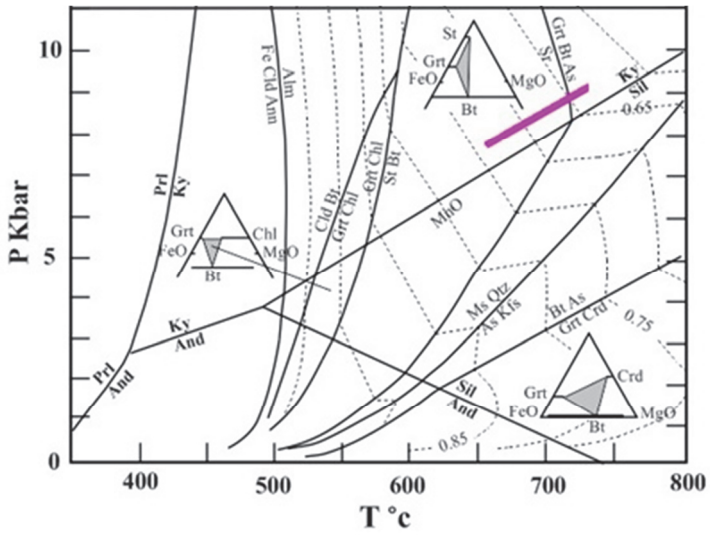

Fig. 19. P-T chart for all types of metasedimentary rocks from Speer and Peacock (1989) and Speer (1995). Isoplates Fe/(Fe + Mg) ratio in garnet at the assemblage containing garnet + biotite. The AFM charts show the stable assemblage in each P-T range.

6. Discussion

The Zagros orogen in the southwestern and southern part of Iran was a result of the convergence between the Arabia and Cimmerian blocks. These blocks rifted away from north of Gondwana at the end of the Palaezoic and were accreted to Eurasia during the Cretaceous (Sheikholeslami 2015). This orogen preserves a record of the deformation history related to the Neotethys evolution, from early rifting, through subduction to final collision (Agard et al. 2011). The Sanandaj-Sirjan zone is bounded by the Zagros main thrust at the southwest and the Urmia-Dokhtar magmatic assemblage to the northeast. This zone is characterized by deformed metamorphic rocks which are associated with numerous plutons and a widespread Mesozoic volcanism (Mohajjel et al. 2003).

The main lithologies, namelygarnet-staurolite schists and garnet schists, in Bahram-Gur complex, east southern of Sanandaj-Sirjan zone represent medium grade metamorphic rocks.

The garnet metamorphic zone in both of garnet schist (HRS-2, HRS-17) and staurolite zone in staurolite garnet schist (HRS-220) are equivalent to amphibolite facies and their protolith is semi-pelitic rocks.

The amounts of SiO_2, TiO_2, Al_2O_3, Fe_2O_3 (total) MgO, CaO Na_2O and K_2O oxides, respectively, are due to the presence in the rocks of quartz, ilmenite, garnet, staurolite, biotite and chlorite, plagioclase and muscovite, respectively.

Generally, minor elements (with the exception of Ni, Zn, V, Cr, and Zr) have high contents in the samples. The high amounts of Ba, Rb and Ce in the metasediments are related to the presence of biotite and muscovite (Table 7).

The amount of manganese oxide in the HRS-220 sample is reduced in samples HRS-17 and HRS-2.

The metasediments exhibit varying classification using different schemes, which may be due to the metasediment supply from different sources. The source rock of metasediments probably is sandstone containing clay matrix with different compositions which can contain higher levels of Fe and Mg. Also, sample HRS-220 is sodic sandstone maybe because of alteration.

According to Bhattia and Crook, (1986); McLennan et al. (1993) and Holail et al. (1998), incompatible elements such as Zr, Nb and Y are mostly enriched in felsic igneous rocks relative to mafic igneous rocks and are not affected during igneous processes.

REE patterns for the metasediment samples. (a) Chondrite-normalized REE plots showing a UCC pattern, (b) UCC-normalized REE patterns are almost similar to UCC. Sources: chondrite (Sun, McDonough 1989), UCC (Taylor, McLennan, 1985).

The rare-earth elements (REE) pattern normalized to chondrite (Sun, McDonough 1989) shows depletion in Eu and high values of the LILE / HFSE and LREE / HREE ratios.

The relatively high amount of Zr, negative Eu anomalies and high LREE/HREE points to a felsic source of the sediments (Armstrong-Altrin et al. 2015), almost similar to upper continental crust.

Our geochemical study of the metasedimentary rocks shows that primary concentrations and ratios of the most petrogenetically important elements in these rocks were not changed during metamorphism, which reached amphibolite facies. This fact allows us to use the distribution of these elements for geodynamic and sedimentological reconstructions (Ivan et al. 2001).

Major and particularly trace element distributions including REEs in the metasedimentary rocks indicates that their clastic protolith was petrographically close to greywackes, with an average content of quartz. The identical source area and homogeneous composition of the protoliths of the metasediments are documented by the small variation in most of the discrimination graphs.

The REE patterns of the metasediments of the Bahram-Gur complex, and the results of discrimination based on other elements with limited fractionation during weathering, transport and sedimentation, indicate an acid or acid/intermediate magmatic source and ensialic island arc provenance of sedimentation which were then metamorphosed into garnet schists and garnet staurolite schists during Neotethys subduction beneath the Iranian plate in the Sanadaj - Sirjan zone.

The results of the multi-equilibrium calculations (Table 10) are consistent with the other methods described in this study and according to PT-Quick, Thermocalc calculations and P-T graph 19, in the presence of staurolite, the stability range of X_{Fe} garnet is limited to 1.87 to temperatures between 600 and 750°C and pressure of 5 to 7.5 kbar. They plot in a compact field near the 45 mw/m^2 continental geotherm. These temperatures and pressures show that the setting for the Cimmerian Orogeny in the southeast Sanandaj – Sirjan Zone is thus considered to reflect a developing active continental margin with deformation and uplift of amphibolite facies metamorphic rocks and early stage of magmatism and metamorphism in the formation of the Neotethys Ocean along the Sanandaj - Sirjan Zone.

The intense deformation and metamorphism in the Bahram-Gur Complex is attributed to convergence along the southwest margin of the Central Iranian microcontinent following

subduction initiation. Thus the Cimmerian Orogeny in the southeastern margins of the Sanandaj–Sirjan Zone is a consequence of Paleo-Tethyan closure (Fergusson et al. 2016).

TABLE 10

Summarizes the results of the thermo-barometry data of the Garnet-Staurolite schist of the Bahram-Gur complex in the SE Sanandaj-Sirjan zone.
* Based on the thermometry Ti diagram against Mg/(Mg + Fe)

Calibration Samples	HRS-220			
	Garnet Staurolite Schist			
T (^{o}C) Ti in Biotite				
Henry et al. (2005)		454	602	
Henry et al. (2005)*		~450	~610	
T (^{o}C) Garnet-Biotite				
Bhattacharya et al. (1992) HW	692.54	682.16	652.01	637.29
Bhattacharya et al. (1992) GS	698.98	687.53	655.15	639.41
Dasgupta et al.(1991)	787.18	762.95	724.63	709.41
Ferry and Spear(1987)	789.05	767.13	709.35	679.43
Hodges and Spear(1982)	810.53	789.84	731.48	707.47
Perchuk and Lavrenteva (1983)	687.19	677.36	650.41	635.83
Thompson (1976)	750.97	735.64	694.37	672.49
Holdaway and Lee(1977)	711.07	698.23	663.42	644.81
Average T of GB (oC)	740.94	725.10	685.10	665.77
P(Kbar)	Core			Rim
GPMB-Mg	7.64	7.57	6.92	7.43
Grs + Prp + Ms = 3An + Phl				
GPMB-Fe	5.99	5.94	5.41	6.12
Grs + Alm + Ms = 3An + Ann				
Average calculated P(kbar)	6.82	6.75	6.16	6.77

7. Conclusions

Geochemistry, mineral chemistry and geothermobarometry of metasediments from the Bahram-Gur complex in the southeastern of Sanandaj-Sirjan zone led to the following conclusions:

- The metasediments of the Bahram-Gur complex are garnet-staurolite schists and garnet schists that belong to two different subunits in the area.
- Two metamorphic phases, S_0 and S_1, in the garnet schists can be distinguished. S_1 has been developed by quartz, muscovite and biotite, and relict of S_0 by garnet, quartz and opaque minerals.

The metamorphic phase S_1 in the garnet-staurolite schists is visible due to the orientation of the muscovite, biotite, chlorite and quartz minerals.

- The protolith of the metasedimentary rocks were greywackes of ensialic island arc provenance derived from an acidic/intermediate magmatic source.

- Abundance of relatively immobile elements (REE, HFSE) in metasediments reflects their original distribution in the magmatic or sedimentary protolith. No significant chemical change caused by metamorphic processes has been found.
- Reviewing the chondrite normalized REE plots, higher concentrations of LREE than HREE with a negative Eu-anomaly represent the rocks due to the influence of the continental crustal components.
- The mineral chemistry of the garnet schists and garnet staurolite schists shows that the plagioclase is in the oligoclase-andesine range. The garnets in the garnet-staurolite schist are rich in almandine and pyrope, while in the garnet schists the almandine is higher than the other end-members of the garnet. The staurolites are richer in Fe than Mg. The biotites have eastonite to siderophyllite components. The muscovites have high Al_2O_3 and low FeO_T contents. The XFe of chlorites decreases with increasing degrees of metamorphism.
- According to the garnet-biotite, GPBMQ and Ti in biotite geothermobarometric methods, also PT-Quick and Thermocalc software, the pressure and temperature ranges are 5-7.5 kbar and 600-750°C along a 45 mw/m^2 geothermal gradient, which can be considered as Barrovian metamorphism, in the form of high pressure amphibolite facies, in the formation of the Neotethys ocean along the Sanandaj-Sirjan Zone of the Zagros orogen.

Acknowledgements. This paper is from the Ph.D. thesis of the first author in the Shahid Bahonar University of Kerman, Iran. The authors would like to thank Dr. Mohssen Moazzen who greatly helped in improving this paper and Dr. Bahram Bahrambygi for supporting the editing of this paper.

8. References

Agard, P., Omrani, J., Jolivet, L., Whitechurch, H., Vrielynck, B., Spakman, W., Monie, P., Meyer, B., & Wortel, R. (2011). Zagros orogeny: a subduction-dominated process. *Geological Magazine, 148*(5-6), 692-725. DOI: https://doi.org/10.1017/S001675681100046X.

Alavi, M. (1994). Tectonics of the Zagros orogenic belts of iran: new data and interpretation. *Tectonophysics, 229*, 211-238:DOI. https://doi.org/10.1016/0040-1951(94)90030-2.

Armstrong-Altrin, J. S. (2015). Evaluation of two multidimen-sional discrimination diagrams from beach and deep-sea sediments from the Gulf of Mexico and their application to Precambrian clastic sedimentary rocks. *International Geology Review, 57*(11-12),1444-1459. DOI: https://doi.org/ 10.1080/00206814.2014.936055.

Barker, A. (1990). Introduction to metamorphic textures and microstructures: Blackie, New York, 162. Bozyazı ve Anamur Arasındaki Bölgenin Jeolojisi: MTA Rep, 82.

Berberian, M., & King, G. (1981). Towards a paleogeography and tectonic evolution of Iran. *Canadian Journal of Earth Sciences, 18*(2), 210-265. DOI: https://doi.org/10.1139/e81-019.

Berberian, F., & Berberian, M. (1981). Tectono-plutonic episodes in Iran. In: Gupta, H.K., Delany, F.M. (Eds.), Zagros Hindukosh, Himalaya Geodynamic Evolution, American Geophysical Union, Washington, DC, 5-32.

Bhattacharya, A., Mohanty, L., Maji, A., Sen, S. K., & Raith, M. (1992a). Non-ideal mixing in the phlogopiteannite binary: constraints from experimental data on Mg-Fe partitioning and a reformulation of the biotite-garnet geothermometer. *Contributions to Mineralogy and Petrology, 111*, 87-93. DOI: 10.1007/BF00296580.

Bhattacharya, A., Mohanty, L., Maji, A., Sen, S. K., & Raith, M. (1992b). Non-ideal mixing in the phlogopiteannite binary: constraints from experimental data on Mg-Fe partitioning and a reformulation of

the biotite-garnet geothermometer. *Contributions to Mineralogy and Petrology, 111*, 87-93. DOI: 10.1007/BF00296580

Bhatia, M. R. (1983). Plate tectonics and geochemical composition of sandstones. *Journal of Geology, 92*,181-193.

Bhatia, M. R., & Crook, K. W. (1986). Trace element characteristics of greywackes and tectonic setting discrimination of sedimentary basins. *Contributions to Mineralogy and Petrology, 92,* 181-193. DOI: https://doi.org/10.1007/BF00375292.

Bucher, K., &Fery, M. (1994). Petrogenesis of Metamorphic Rocks. 6thedition.Springer-Verlag, Berlin, 318 pp.

Bucher, K., & Grapes, R. (2011). Petrogenesis of Metamorphic Rocks. Springer-Verlag Berlin Heidelberg, 441 p.

Cope, T., Ritts, B. D., Darby, B. J., Fildani, A., & Graham, S. A. (2005). Late Paleozoic sedimentation on the Northern margin of the North China Block: implications for regional tectonics and climate Change. *International Geology Review, 47*, 270-296 :DOI .https://doi.org/10.2747/0020-6814.47.3.270.

Dasgupta, S., Sengupta, P., Guha, D., & Fukuoka, M. (1991). A refined garnet-biotite Fe− Mg exchange geothermometer and its application in amphibolites and granulites. Contributions to *Mineralogy and Petrology, 109*(1), 130-137. DOI: https://doi.org/10.1007/BF00687206.

Deer, W., Howie, R. & Zussman, J. (1996). The rockforming minerals Vol 5: Nonsilicates, Apatite: New York: Londman.

Degraaff-surpless, K., Graham, S. A., Wooden, J. L., & McWiliams, M. O. (2002). Detrital zircon provenance analysis of the Great Valley Group, California: evolution of an arc-fore arc system. *Geology Society of American Bulltain 114*, 1564-1580 DOI:https://doi.org/10.1130/0016-7606(2002)114<1564:DZPAOT>2.0.CO;2.

Dickinson, W.R. (1970). Interpreting detrital modes of graywacke and arkose. *Journal of Sedimentary Petrology, 40,* 695-707.

Dickinson, W.R. (1985). Interpreting provenance relation from detrital modes of sandstone. In Zuffa, G.G. (ed). Provenance of Arenites: NATO ASI Series, C148, D. Reidel Publishing Company, Dordrecht, 333-363.

Dymek, R. F. (1983). Titanium, aluminum and interlayer cation substitutions in biotite from high-grade gneisses' West Greenland. American Mineralogist, 6, 880-399.

Engel, A. J., & Engel, C. G. (1960). Progressive Metamorphism and Granitizationof The Major Paragniess, Northwest Adirondack Mountains, New York: Part II: Mineralogy. Geological society of America bulletin, 71(1), 1-58.

Fergusson, C. L., Nutman, A. P., Mohajjel, M., & Bennett, V. C. (2016). The Sanandaj–Sirjan Zone in the Neo-Tethyan suture, western Iran: Zircon U–Pb evidence of late Palaeozoic rifting of northern Gondwana and mid-Jurassic orogenesis. *Gondwana Research, 40*, 43-57. DOI: https://doi.org/10.1016/j.gr.2016.08.006.

Ferry, J. t., & Spear, F. (1987). Experimental calibration of the partitioning of Fe and Mg between biotite and garnet. *Contributions to Mineralogy and Petrology, 66*(2), 113-117. DOI: https://doi.org/ 10.1007/BF00372150.

Floyd, P. A., & Leveridge, B. E. (1987). Tectonic environment of the Devonian Gramscatho basin, south Cornwall: framework mode and geochemical evidence from turbiditic sandstones. Journal of Geological Society of London, 144: 531-542.

Floyd P.A., Winchester J.A., & Park R.G. (1989). Geochemistry and tectonic setting of Lewisian clastic metasediments from the early Proterozoic Loch Maree Group of Gairloch, N. W. Scotland. *Precambrian Research 45*, 203-214. DOI: https://doi.org/10.1016/0301-9268(89)90040-5.

Ghazi, J.M., & Moazzen, M. (2015). Geodynamic evolution of the Sanandaj-Sirjan zone, Zagros Orogen, Iran. *Turkish Journal of Earth Sciences, 24*(5), 513-528. DOI: doi:10.3906/yer-1404-12.

Henry, D. J., Guidotti, C. V., & Thomson, J. A. (2005). The Ti-saturation surface for low-to-medium pressure metapelitic biotites: Implications for geothermometry and Ti-substitution mechanisms. *American Mineralogist, 90*(2-3), 316-328. DOI: https://doi.org/10.2138/am.2005.1498.

Henry, D.J., & Guidotti, C.W. (2002). Ti in biotite from metapelitic rocks: temperature effects, crystallochemical controls, and petrologic applications. *American Mineralogist, 87*, 375-382.

Herron, M. M. (1988). Geochemical classification of terrigenous sands and shales from core or log data. *Journal of sedimentary Petrology, 85*, 820-829. DOI: https://doi.org/10.1306/212F8E77-2B24-11D7-8648000102C1865D.

Hodges, K., & Spear, F. S. (1982). Geothermometry, geobarometry and the Al_2SiO_5 triple point at Mt. Moosilauke, New Hampshire. *American Mineralogist, 67*(11-12), 1118-1134.

Hoisch, T. D. (1991). Equilibria within the mineral assemblage quartz+ muscovite+ biotite+ garnet+ plagioclase, and implications for the mixing properties of octahedrally-coordinated cations in muscovite and biotite. *Contributions to Mineralogy and Petrology, 108*(1-2), 43-54. DOI: https://doi.org/10.1007/BF00307325.

Holail, H.M., & Moghazi, A.M. (1998). Provenance, tectonic setting and geochemistry of greywackes and siltstones of the Late Precambrian Hammamat Group, Egypt. *Sedimentary Geology 116,* 227-250. DOI: https://doi.org/10.1016/S0037-0738(97)00104-8.

Holdaway, M.J. (2001). Recalibration of the GASP geobarometer in light of recent garnet and plagioclase activity models and versions of the garnet-biotite geothermometer. *American Mineralogist, 86*, 1117-1129. DOI: https://doi.org/10.2138/am-2001-1001 Holdaway, M., & Lee, S. M. (1977). Fe-Mg cordierite stability in high-grade pelitic rocks based on experimental, theoretical, and natural observations. *Contributions to Mineralogy and Petrology, 63*(2), 175-198.

Holland, T.J.B., & Powell, R. (1985). An internally consistent thermodynamic dataset with uncertainties and correlations: 2. Data and results. *Journal of Metamorphic Geology, 3*, 343-370.

Holland, T.J.B., & Powell, R. (1998). An internally consistent thermodynamic data set for phases of petrological interest: *Journal of Metamorphic Geology, 16*(3), 309-343. DOI: https://doi.org/10.1111/j.1525-1314.1998.00140.x.

Hooper, R. J., Baron, I., Hatcher, J. R. R. D., & Agah, S. (1994). The development of the southern Tethyan margin in Iran after the breakup of Gondwana: implications of the Zagros hydrocarbon province. *Geosciences, 4*, 72-85.

Horton, B.K., Hassanzadeh, J., Stockli, D.F., Axen, G.J., Gillis, R.J., Guest, B., Amini, A., Fakhari, M., Zamanzadeh, S.M., & Grove, M. (2008). Detrital zircon provenance of Neoproterozoic to Cenozoic deposits in Iran: implications for chronostratigraphy and collisional tectonics. *Tectonophysics, 451*(1-4), 97-122. DOI: 10.1016/j.tecto.2007.11.063

Ivan, P., Meres, s., Putis, M., & Kohut, M. (2001). Early Paleozoic metabasalts and metasedimentary rocks from the Male Karpaty MTS (Western Carpathians): evidence for rift basin and ancient oceanic crust. *Geologica* CARPATHICA, 52, 2, BRATISLAVA, 67-78.

Kwak, T. A. (1968). Ti in biotite and muscovite as an indication of the metamorphic grade in almandine amphibolite facies rocks from Sudbury, Ontario. *Geochimica et Cosmochimica Acta, 32*(11), 1222-1229. DOI: https://doi.org/10.1016/0016-7037(68)90124-5.

Maas, R., & McCulloch, M.T. (1991). The provenance of Archean clastic metasediments in the Narryer Gneiss Complex, Western Australia: Trace element geochemistry, Nd isotopes and U–Pb ages for detrital zircons. *Geochimica et CosmochimicaActa, 55*, 1915-1932 :DOI .https://doi.org/10.1016/0016-7037(91)90033-2.

McLennan, S. M. (2001). Relationships between the trace element composition of sedimentary rocks and upper continental crust. *Geochemistry Geophysics Geosystems 2*, DOI: https://doi.org/10.1029/2000GC000109 McLennan, S.M., Hemming, S., McDaniel, D.K., & Hanson, G.N. (1993). Geochemical approaches to sedimentation, provenance and tectonics. In: Johnsson, M.J., Basu, A. (Eds.), Processes Controlling the Composition of Clastic Sediments, vol. 284. Geological Society of America, Special Paper, pp. 21-40.

Miyashiro, A. (1973). Metamorphism and Metamorphic Belts. G. Allen and Unwin, London, pp. 492.

Mohajjel, M., & Fergusson, C. L. (2014). Jurassic to Cenozoic tectonics of the Zagros Orogen in northwestern Iran. *International Geology Review, 56*, 263-287. DOI: 10.1080/00206814.2013.853919.

Mohajjel, M., Fergusson, C., & Sahandi, M. (2003). Cretaceous–Tertiary convergence and continental collision, Sanandaj–Sirjan zone, western Iran. *Journal of Asian Earth Sciences, 21*(4), 397-412. DOI: https://doi.org/10.1016/S1367-9120(02)00035-4.

Newton, R.C., & Haselton, H.T. (1981). Thermodynamics of the garnet-plagioclase-Al2SiO5-quartz geobarometer. In: Newton R.C. (Ed.). Thermodynamics of Minerals and Melts: New York (Springer-Verlag), p.131-147. Ky version of the GASP geobarometer; expressions are taken from the GPT MS Excel program of J.Reche & F.J.Martinez (1996).

Passchier, C. W., & Trouw, R. A. (2005). Microtectonics (Vol. 1): Springer Science & Business Media, 366 pp.

PatiñoDouce, A. E. (1993). Titanium substitution in biotite: an empirical model with applications to thermometry, O_2, and H_2O barometries, and consequences form biotite stability. *Chemical Geology, 108*, 133-162. DOI: https://doi.org/10.1016/0009-2541(93)90321-9.

Perchuk, L., & Lavrent'Eva, I. (1983). Experimental investigation of exchange equilibria in the system cordierite-garnet-biotite. Kinetics and equilibrium in mineral reactions (pp. 199-239): Springer.

Rieder, M., Cavazzini, G., D'yakonov, Y. S., Frank-Kamenetskii, V. A., Gottardi, G., Guggenheim, S., . . . Radoslovich, E. W. (1998). Nomenclature of the micas. *Clays and clay minerals, 46*(5), 586-595. DOI: https://doi.org/10.1346/CCMN.1998.0460513.

Robert, J.L. (1976). Titanium solubility in synthetic phlogopite solid solutions. *Chemical Geology, 17,* 213-227. DOI: https://doi.org/10.1016/0009-2541(76)90036-X.

Roser, B. P., & Korsch, R. J. (1988). Provenance signatures of sandstone-mudstone suites determined using discriminant function analysis of major-element data. *Chemical Geology,67*, 119-139 .DOI: https://doi.org/10.1016/0009-2541(88)90010-1.

Sabzehi, M. (1997). Geological map of GolGohar, 1/100000. Geological Survey of Iran.

Shahabpour, J. (2005). Tectonic evolution of the orogenic belt in the region located between Kerman and Neyriz. *Journal of Asian Earth Sciences, 24*, 405-417. DOI: https://doi.org/10.1016/j.jseaes.2003.11.007.

She, Z. B., Ma, C. Q., Mason, R., Li, J. W., Wang, G. C., & Lei, Y. H. (2006). Provenance of the Triassic Songpan -Ganzi flysch, west China. *Chemical Geology 231,* 159-175. DOI: 10.1016/j.chemgeo.2006.01.001.

Sheikholeslami, M.R. (2015). Deformations of Palaeozoic and Mesozoic rocks in southern Sirjan,Sanandaj‐Sirjan Zone, Iran. *Journal of Asian Earth Sciences 106*, 130-149. DOI: https://doi.org/ 10.1016/j.jseaes.2015.03.007.

Spear, F. S. (1993). Metamorphic phase equilibria and pressure-temperature-time paths (Vol. 1): Mineralogical Society of America Washington, DC, 799 p., ISBN 0-939950-34-0.

Spear, F. S., & Peacock, S. M. (1989). Metamorphic pressure-temperature-time paths. American Geophysical Union, Washington, D. C. 102 p.

Sun, S. S., & McDonough, W. F. (1989). Chemical and isotopic systematics of oceanic basalts: implications for mantle composition and processes. In: Saunders, A.D., Norry, M.J. (Eds.), Magmatism in the Ocean Basins. Geological Society of London Special Publication, 42, 313-345.

Sun, W. H., Zhou, M. F., Yan, D. P., Li, J. W., & Ma, Y. X. (2008). Provenance and tectonic setting of the Neoproterozoic Yanbian Group, western Yangtze Block (SW China)". *Precambrian Research 167, 213-236*. DOI:10.1016/j.precamres.2008.08.001.

Taylor, S.T., & McLennan, S.M. (1985). The Continental Crust: its Composition and Evolution. Blackwell Scientific, Oxford.

Tatsumi, Y., & Eggins, S. (1995). Subduction Zone Magmatism". Blackwell Science, Cambridge, MA 211pp.

Thompson, P. (1976). Isograd patterns and pressure-temperature distributions during regional metamorphism. *Contributions to Mineralogy and Petrology, 57*(3), 277-295. DOI: https://doi.org/10.1007/BF03542938.

Totten M.W., Hanan M.A., & Weaver B.L. (2000). Beyond the whole-rock geochemistry of shales:The importance of assessing mineralogic controls for revealing tectonic discriminants of multiple sediment sources for the Ouachita Mountain flysch deposits. *Geological Society of America Bulletin, 112*, 1012-1022. DOI: https://doi.org/10.1130/0016-7606(2000)112<1012:BWGOST>2.0.CO;2.

Wu, C.M (2015a). Revised empirical garnet-biotite-muscovite-plagioclase geobarometer in metapelites. *Journal of Metamorphic Geology, 33*(2), 167-176. DOI:10.1111/jmg.12115.

Wu, C.M., Zhang, J., & Ren, L.D. (2004a). Empirical Garnet-Biotite-Plagioclase-Quartz (GBPQ) Geobarometry in Medium- to High-Grade Metapelites. *Journal of Petrology, 45*(9), 1907-1921. DOI:10.1093/petrology/egh038.

Wu C.M., Zhao G.C. (2007a). The metapelitic garnet-biotite-muscovite-aluminosilicate-quartz (GBMAQ) geobarometer. *Lithos, 97*(3-4),.365-372. DOI:10.1016/j. lithos.01.003.